Exploring the Atmosphers of Ultra-hot Jupiters using *TESS* Phase Curves

Jenna Bittner
Anusha Pai Asnodkar, Marshall Johnson, Kaz Gary

July 2024

1 Abstract

Ultra-hot Jupiters are a class of exoplanets similar in mass and size to Jupiter. They are extreme environments with unique properties and atmospheric conditions absent in our Solar System. These conditions can be studied to deepen our understanding of atmospheric physics and chemistry, and in this paper I use phase curves to do so. Phase curves are a method used to study exoplanets that show the light they reflect and emit during a full orbit. They reveal information about the planet's atmosphere, specifically heat distribution, wind circulation, and potential presence and composition of clouds. In this paper I adopt the methods used in Wong et al. 2020. I clean the light curves of bad data, normalize, and phase-fold them. I create a model with an analytical combination of sinusoidal harmonics, and fit the model to the light curve data using Bayesian parameter estimation. Of the best-fit parameters, delta is of particular interest. It indicates a phase curve offset, which suggest the presence of equatorial jets in the atmosphere. The sample of exoplanets I study are KELT-9b, KELT-20b, TOI-1431b, TOI-1518b, WASP-76b, WASP-12b, and MASCARA-1b, chosen because *PEPSI* spectroscopic data is available on them. Their relevant stellar and planetary parameters are listed in table 1. I study their phase curves to determine if equatorial jets are present in their atmospheres, and find that they are present in each atmosphere. This work will feed into a larger population-level analysis of ultra-hot Jupiter atmospheres combining photometric and spectroscopic data to piece together a holistic picture of their atmospheric dynamics and composition.

Planetary Values			
Planet	Equilibrium Temperature (K)	Mass (M_J)	Radius (R_J)
KELT-9b	4050	2.88	1.891
KELT-20b	2262	3.382	1.741
TOI-1431b	2370	3.12	1.49
TOI-1518b	2492	2.3	1.875
WASP-76b	2228	0.894	1.854
WASP-12b	2592	1.465	1.937
MASCARA-1b	2594	3.7	1.597
Stellar Values			
Host Star	Effective Temperature (K)	Spectral Type	
KELT-9	9550	B	
KELT-20	9032	A	
TOI-1431	7690	A	
TOI-1518	7300	A	
WASP-76	6366	F	
WASP-12	6154	F	
MASCARA-1	7490	A	

Table 1: Summary of planetary and stellar values

2 Background

2.1 Phase curves

Phase curves represent the combined brightness of a planet and its star and how they both change over the course of one orbit. They provide insight on the atmospheres of planets, specifically heat distribution, wind circulation, and the potential presence and composition of clouds. The term phase curve is used in a similar sense as the phases of the Moon because exoplanets also display phases. Phases of an exoplanet are defined by their orbital position with respect to observer's perspective. The planet is most luminous before and after secondary eclipse, when the planet passes behind the star. This corresponds to the brightest part of the phase curve. The planet is least luminous before and after transit, when the planet crosses in front of the star. This corresponds to the dimmest part of the phase curve. Since brightness correlates with temperature, the brightest and dimmest parts of the phase curve correspond to the hottest and coolest points on the planet, respectively. This brightness variation modulates with a periodicity that matches the orbital period of the planet (Parmentier and Crossfield 2017).

2.2 Ultra-hot Jupiters

Exoplanets similar in mass and size to Jupiter, yet with extreme proximity to their host stars, are known as ultra-hot Jupiters. This proximity produces numerous interesting consequences. They have small orbital periods of less than 10 days, and are tidally-locked, resulting in a very hot permanent day side and a cooler night side. The day side of these planets reach temperatures greater than 2200 K. Additionally, these exoplanets are known to have non-negligible gravitational effects on their host stars.

2.3 Ellipsoidal variations

Due to their mass and proximity to their hosts, ultra-hot Jupiters can distort the shape of their star. As the planet orbits, the star is pulled into a teardrop shape, with the point of the teardrop being closest to the planet and following it around as it orbits. To the observer, this produces a larger cross section on the star when the planet is at either greatest elongation, and a smaller cross section during transit and secondary eclipse. The star's flux will vary along with its cross section, and thus produce fluctuations in the star's contribution to the phase curve. This modulates with twice the frequency of the planet's orbit, making it distinguishable from the planet's brightness modulation (Shporer 2019).

2.4 Doppler beaming effect

Similar to ellipsoidal variations, the Doppler beaming effect is a result of an ultra-hot Jupiter's non-negligible gravitational effects on its host star. For these systems, the star's motion around the barycenter is more significant and the relativistic Doppler effect is notable. As the star moves towards the observer, its light is blue shifted, and this occurs approximately around eastern quadrature. As the star moves away from the observer, its light is red shifted, and this occurs around western quadrature. This change in flux has a periodicity that matches the orbital period of the planet, but is distinguished by the planet's brightness modulation by an offset in phase of $\pi/2$ (Shporer 2019).

3 Methodology

3.1 TESS light curves

The phase curves I use are from *TESS*, an all-sky survey to detect transiting exoplanets. This space telescope is a NASA mission led by MIT that finds and monitors all types of objects that change in brightness, from nearby asteroids to pulsating stars and distant galaxies containing supernovae. It's primary purpose is to monitor stars for temporary dips in brightness caused by transiting exoplanets, and since its launch in April of 2018, it has detected over 7000 candidate exoplanets, almost 500 of which have been confirmed. (Ricker et al. 2014) Light curves are extracted from *TESS* sky images through aperture photometry, in which an aperture is defined containing the target star, and the flux from each pixel is summed together to produce a single flux value for the star. This is repeated for many images at regular cadences, and I use 2-minute cadence data. I use *TESS* Pre-search Data Conditioning SAP (PDCSAP) flux, data from which long term trends have been removed using co-trending basis vectors. *TESS* observes the sky in different angular slices, referred to as sectors. Each sector is observed for two orbits of the satellite around Earth, about 27 days on average. The following table lists the sectors of data available for each planet.

Planet	*TESS* Sectors Available
KELT-9b	14, 15, 41, 55, 75
KELT-20b	14, 40, 41, 54, 74, 75
TOI-1431b	15, 16, 55, 56, 57, 76, 77
TOI-1518b	57, 58, 77
WASP-76b	30, 42, 43
WASP-12b	20, 43, 44, 45, 71, 72
MASCARA-1b	55

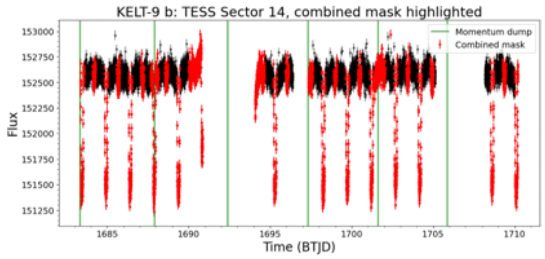

Figure 1: The light curve is the black data points. The combined mask to be removed is highlighted in red. It includes bad data quality flags from the *TESS* pipeline, flux ramps, secondary eclipses, transits, and data around momentum dumps. The vertical green lines are momentum dumps.

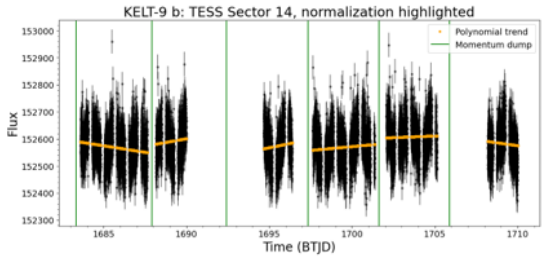

Figure 2: The light curve is the black data points. For long term detrending, the best-fit-low order-polynomial is the orange line. The vertical green lines are momentum dumps.

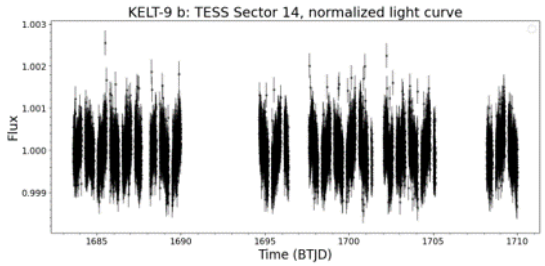

Figure 3: The light curve is the black data points, it is the light curve after the combined mask is removed and best-fit-low-order polynomial is divided out.

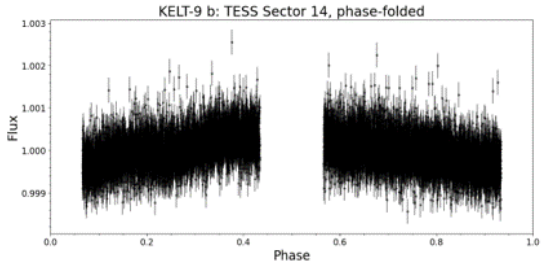

Figure 4: The light curve in black is phase folded over orbital period. The gap at phase=0.5 is where secondary eclipse occurs, the gap at phase=0 and phase=1 is where transit occurs.

Figure 5: Lightcurves of KELT-9b Sector 14 to highlight important steps in data cleaning process.

3.2 Data cleaning

TESS light curves contain numerous interesting features. Some of these are astrophysical and others are systematics that must be removed. In *TESS* PDCSAP data, systematics from noise sources such as scattered light and instrumental effects are corrected, and egregiously bad data points are removed or set to Nan (not a number). I remove all of these values associated with bad data quality flags. I remove data around momentum dumps because they can cause discontinuities in flux. Since the phase curve signal of interest is the planet's atmospheric brightness modulation, I remove data around secondary eclipses and transits because they dominate and obscure the planet's relatively faint signal. Lastly, I remove flux ramps based on personal judgment. These are any unaccounted for sudden rises or falls that are not likely to be astrophysical. I detrend the light curve by finding the best-fit-low-order polynomial for each segment of data within momentum dumps. I select the order of the polynomial so as to remove any long term trends caused by instrumental effects without removing any short timescale variations that are important features of the planet's atmospheric brightness modulation. Once the light curves are cleaned and normalized, I phase-fold them over the period. This folds all of the individual orbits from the light curve on top of one another, resulting in one cycle of modulation over the planet's orbital period. On these phase-folded light curves, the secondary eclipses and transits will be masked out, so there will be gaps. Regardless, the brightness should peak near secondary eclipse (phase 0.5), as this is when the planet's entire day side is facing us. Likewise, the dimmest part of the phase curve should be at transit (phase 0 and 1), because this is when the planet's night side is facing us. Each of these steps are done for each individual *TESS* sector of data (Wong et al. 2020).

3.3 Phase curve modeling

The light curve model is an analytical combination of sinusoidal harmonics, and it receives contributions from the planet's phase curve, ellipsoidal variations, the Doppler beaming effect, and stellar pulsations. The description of each variable can be found in Table 3. The equation for the total light curve model is below (Wong et al. 2020).

$$\psi_{\rm tot}(t) = \frac{\psi_*(t)\Theta(t) + \psi_p(t)}{1 + \overline{f_p}} \tag{1}$$

The first contribution to the total light curve is from the planet's phase curve. It contributes a cosine component, since it is minimum at phase 0. The period matches the orbital period of the planet. The following equation is for the planetary phase curve component (Wong et al. 2020).

$$\psi_p(t) = \overline{f_p} + B_1 \cos(2\pi\phi + \delta) \tag{2}$$

$$\text{where } \phi = \tfrac{t-t_0}{P}$$

Stellar harmonics are the next light curve contributions. Ellipsoidal variations contribute a cosine component because it is minimum at phase 0. The period is twice the frequency of the planet's orbital period. Doppler beaming contributes a sine component because it is 0 at phase 0. The period matches the orbital period of the planet. The equation for stellar harmonics consists of two summations. I will go up to the first 3 harmonics, as seen below (Wong et al. 2020).

$$\begin{aligned}\psi_*(t) = 1 &+ A_1 \sin(2\pi\phi) \\ &+ A_2 \sin(4\pi\phi) + B_2 \cos(4\pi\phi) \\ &+ A_3 \sin(6\pi\phi) + B_3 \cos(6\pi\phi) \end{aligned} \quad (3)$$

Stellar pulsations are the final contribution, and they only pertain to KELT-9b, as KELT-9 is the only star in which pulsations were detected. For the other exoplanets in the sample, the stellar pulsations component is removed. They contribute both a sine and cosine component. The period is much smaller that the planet's orbital period, producing small fluctuations in the total light curve. The following equation is the stellar pulsations component (Wong et al. 2020).

$$\Theta(t) = 1 + \alpha \sin(2\pi\xi) + \beta \cos(2\pi\xi) \quad (4)$$

$$\text{where } \xi = \tfrac{t - t_0}{\Pi}$$

To fit the multi-component model to the *TESS* light curves I use Bayesian parameter estimation. The Bayesian approach estimates parameter values by updating a prior belief about model parameters with new evidence. The prior belief is represented by a prior distribution that describes the probability of the parameter having a range of values based on prior information. I use a Gaussian prior for P and t_0, which assigns the highest probability to the mean value, with a Gaussian spread around it. For all other parameters I use a uniform prior, which assigns an equal probability to all values within a specified range. The new data is called a likelihood distribution. It assigns the probability of a parameter having a given value by comparing the resulting model to the data. The parameter value that yields the closest match to the data has the highest probability. This is quantified by the χ^2 function, in which a smaller χ^2 indicates a closer match. Bayes's theorem combines the prior and likelihood probability to determine the posterior probability, the overall probability assigned to a parameter. The next step of Bayesian parameter estimation involves parameter space sampling. This is done through `dynesty`[1] using nested sampling, and it searches the parameter space for the best-fit phase curve parameters and their associated uncertainties. The probability distributions are shown with corner plots, which return all of the best-fit model parameters (Wong et al. 2020).

Variable	Meaning
Equations	
$\psi_{\text{tot}}(t)$	Total light curve model
$\psi_p(t)$	Planetary phase curve model
$\psi_*(t)$	Stellar harmonics model
$\Theta(t)$	Stellar pulsations model
Orbital Parameters	
t_0	Transit time
P	Orbital Period
Phase Curve Parameters	
$\overline{f_p}$	Average flux
B_1	Semiamplitude
δ	Phase shift
Stellar Harmonics Parameters	
A_1	First harmonic semiamplitude
A_2, B_2	Second harmonic semiamplitudes
A_3, B_3	Third harmonic semiamplitudes
Stellar Pulsations Parameters	
Π	Pulsation period
α, β	Semiamplitudes

Figure 6: Meaning of each variable

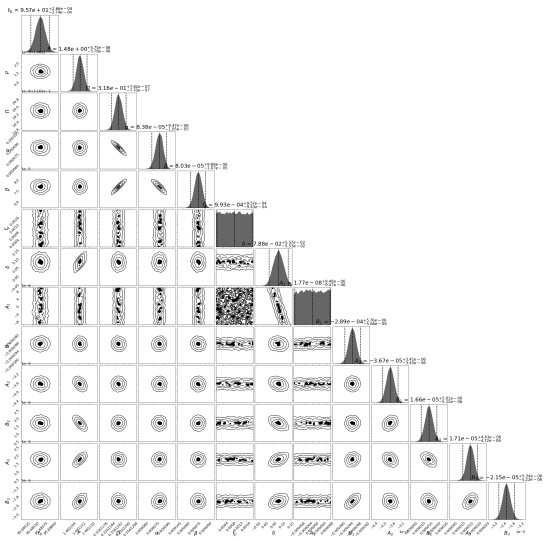

Figure 7: Example corner plot. This is for all sectors of KELT-9b. The top panels show the probability distribution for each parameter, and the best-fit value is above top panel.

[1] Dynesty is a Python package for Bayesian inference using nested sampling, developed by Speagle.

4 Results

The peak of phase curves correspond to the hottest point on planets. They are expected to occur around the time of secondary eclipse because that is when the entire day side of the planet is facing us, and the hotspots are expected to be at the substellar point, the point on the planet closest to the host star. However, the non-zero value of the delta parameter and the position of each phase curve peak suggests otherwise. As seen on each of the phase curves, the peak is slightly offset from phase 0.5, the time of secondary eclipse. This indicates that the hotspot does not coincide with the substellar point. Tidal-locking creates a harsh temperature contrast between the day and night side of the planet, creating super-rotating equatorial jets. Super-rotating implies the jets travel faster than the planet rotates, and equatorial implies they flow along the planet's equator. These jets circulate the planet and redistribute heat, driving the hotspot to be offset longitudinally from the substellar point. WASP-76b and WASP-12 b each have a delta parameter an order of magnitude larger than the other exoplanets, implying their offset was greater. This suggests faster and stronger moving winds. The offset is typically eastward, as jets circulate in the direction of the planet's rotation. A positive, non-zero delta value suggests an eastward offset, as seen with KELT-9b, TOI-1518b, and WASP-76b. A negative delta value suggests a westward hotspot, which is relatively uncommon in ultra-hot Jupiters, and could be caused by unique astmospheric dynamics. In this sample, TOI-1431b, WASP-12b, and MASCARA-1b appeared to have a westward hotspot. I have yet to mention KELT-20b because its delta value suggests an eastward hotspot, but the offset is clearly westward on the phase curve. I attribute this discrepancy to the fact that KELT-20b's delta parameter did not converge, and instead multiple best-fit values were found.

5 Discussion

The future of this project is to improve these models and parameter values, and expand the scope of the study to include an analysis on heat distribution and potential presence and composition of clouds. Not all of the phase curves show a nice curved shape, but they are what I could accomplish in the time given. I would aim to understand what is causing the irregular shapes with those particular light curves and improve them. Additionally, the error bars on the delta parameter are relatively large, so it would be beneficial if that parameter converged better, especially in the case of KELT-20b. The maximum and minimum points on the phase curve indicate how harsh the day-night temperature contrast is. If the contrast is large and the curve is more pronounced, that would suggest poor heat distribution. If the contrast is small and the curve is flatter, that would suggest efficient heat distribution. I will look at the phase curves in different wavelengths, and the presence of clouds will increase the brightness in one of the wavelengths. This specific wavelength will indicate the composition of the cloud, as chemical compounds emit light in particular wavelengths. This analysis will be combined with high-resolution spectroscopy to break the degeneracy between heat recirculation efficiency and albedo. This is a degeneracy in which atmospheric dynamics and clouds can both change the phase offset and amplitude of the planet phase curve in similar ways, so having a direct measurement of the wind speed from spectroscopy can break that degeneracy to get a better constraint on albedo and thus cloud composition.

Parameters	KELT-9b	KELT-20b	TOI-1431b	TOI-1518b
P (days)	$1.48^{+5.78\times10^{-6}}_{-5.57\times10^{-6}}$	$3.47^{+4.34\times10^{-7}}_{-4.23\times10^{-7}}$	$2.65^{+5.71\times10^{-6}}_{-5.82\times10^{-6}}$	$1.90^{+3.14\times10^{-6}}_{-3.15\times10^{-6}}$
t_0 (BTJD)	$95.7^{+2.66\times10^{-4}}_{-2.74\times10^{-4}}$	$2.29\times10^{3}\,^{+2.70\times10^{-4}}_{-2.76\times10^{-4}}$	$1.74\times10^{3}\,^{+2.74\times10^{-4}}_{-2.78\times10^{-4}}$	$1.81\times10^{3}\,^{+2.74\times10^{-4}}_{-2.71\times10^{-4}}$
$\overline{f_p}$ (ppm)	$9.93\times10^{-4}\,^{+9.57\times10^{-4}}_{-9.43\times10^{-4}}$	$9.81\times10^{-4}\,^{+9.66\times10^{-4}}_{-9.31\times10^{-4}}$	$1.05\times10^{-3}\,^{+9.05\times10^{-4}}_{-9.97\times10^{-4}}$	$9.89\times10^{-4}\,^{+9.62\times10^{-4}}_{-9.42\times10^{-4}}$
δ (deg)	$7.88\times10^{-2}\,^{+5.57\times10^{-2}}_{-5.53\times10^{-2}}$	$1.81\times10^{-2}\,^{+3.55\times10^{-1}}_{-3.92\times10^{-1}}$	$-4.53\times10^{-2}\,^{+2.52\times10^{-2}}_{-2.45\times10^{-1}}$	$5.22\times10^{-2}\,^{+7.48\times10^{-2}}_{-7.65\times10^{-2}}$
A_1 (ppm)	$1.17\times10^{-8}\,^{+9.48\times10^{-6}}_{-9.47\times10^{-6}}$	$-3.28\times10^{-6}\,^{+9.30\times10^{-6}}_{-8.56\times10^{-6}}$	$-5.80\times10^{-8}\,^{+9.50\times10^{-6}}_{-9.43\times10^{-6}}$	$-1.21\times10^{-7}\,^{+9.61\times10^{-6}}_{-9.35\times10^{-6}}$
B_1 (ppm)	$-2.89\times10^{-4}\,^{+5.76\times10^{-6}}_{-5.66\times10^{-6}}$	$-2.08\times10^{-5}\,^{+4.43\times10^{-6}}_{-4.72\times10^{-6}}$	$-4.00\times10^{-5}\,^{+3.20\times10^{-6}}_{-3.20\times10^{-6}}$	$-1.64\times10^{-4}\,^{+8.20\times10^{-6}}_{-7.98\times10^{-6}}$
A_2 (ppm)	$-3.67\times10^{-5}\,^{+3.64\times10^{-6}}_{-3.85\times10^{-6}}$	$4.81\times10^{-6}\,^{+3.01\times10^{-6}}_{-2.94\times10^{-6}}$	$1.57\times10^{-6}\,^{+2.74\times10^{-6}}_{-2.71\times10^{-6}}$	$4.79\times10^{-6}\,^{+6.76\times10^{-6}}_{-6.74\times10^{-6}}$
B_2 (ppm)	$1.666\times10^{-5}\,^{+5.01\times10^{-6}}_{-5.12\times10^{-6}}$	$1.47\times10^{-5}\,^{+3.34\times10^{-6}}_{-3.43\times10^{-6}}$	$-1.17\times10^{-5}\,^{+3.06\times10^{-6}}_{-3.06\times10^{-6}}$	$-1.71\times10^{-5}\,^{+7.77\times10^{-6}}_{-7.69\times10^{-6}}$
A_3 (ppm)	$1.71\times10^{-5}\,^{+4.43\times10^{-6}}_{-4.72\times10^{-6}}$	$-6.67\times10^{-7}\,^{+3.10\times10^{-6}}_{-3.10\times10^{-6}}$	$-4.56\times10^{-6}\,^{+2.74\times10^{-6}}_{-2.77\times10^{-6}}$	$4.31\times10^{-6}\,^{+6.83\times10^{-6}}_{-6.65\times10^{-6}}$
B_3 (ppm)	$-2.15\times10^{-5}\,^{+5.34\times10^{-6}}_{-5.22\times10^{-6}}$	$-4.53\times10^{-6}\,^{+3.57\times10^{-6}}_{-3.37\times10^{-6}}$	$6.76\times10^{-7}\,^{+3.12\times10^{-6}}_{-3.18\times10^{-6}}$	$-4.43\times10^{-6}\,^{+8.10\times10^{-6}}_{-8.03\times10^{-6}}$
Π (hr)	$3.16\times10^{-1}\,^{+7.82\times10^{-7}}_{-97.70\times10^{-7}}$	—	—	—
α (ppm)	$8.38\times10^{5}\,^{+9.47\times10^{-6}}_{-1.05\times10^{-5}}$	—	—	—
β (ppm)	$8.03\times10^{-5}\,^{+9.89\times10^{-6}}_{-1.07\times10^{-5}}$	—	—	—

Parameters	WASP-76b	WASP-12b	MASCARA-1b
P (days)	$1.81^{+1.91\times10^{-7}}_{-1.99\times10^{-7}}$	$1.09^{+7.76\times10^{-8}}_{-8.04\times10^{-8}}$	$2.15^{+1.70\times10^{-6}}_{-1.66\times10^{-6}}$
t_0 (BTJD)	$2.37\times10^{3}\,^{+2.80\times10^{-4}}_{-2.79\times10^{-4}}$	$36.7^{+2.55\times10^{-4}}_{-2.952\times10^{-4}}$	$1.83\times10^{3}\,^{+2.73\times10^{-4}}_{-2.74\times10^{-4}}$
$\overline{f_p}$ (ppm)	$1.01\times10^{-3}\,^{+9.34\times10^{-4}}_{-9.65\times10^{-4}}$	$8.84\times10^{-4}\,^{+1.06\times10^{-3}}_{-8.39\times10^{-4}}$	$1.02\times10^{-3}\,^{+9.25\times10^{-4}}_{-9.75\times10^{-4}}$
δ (deg)	$0.142^{+1.07\times10^{-1}}_{-1.06\times10^{-1}}$	$-0.664^{+1.89}_{-6.02\times10^{-1}}$	$-3.09\times10^{-2}\,^{+7.82\times10^{-1}}_{-7.25\times10^{-1}}$
A_1 (ppm)	$1.65\times10^{-8}\,^{+9.46\times10^{-6}}_{-9.50\times10^{-6}}$	$2.49\times10^{-4}\,^{+6.20\times10^{-4}}_{-9.20\times10^{-4}}$	$1.10\times10^{-5}\,^{+9.43\times10^{-5}}_{-9.97\times10^{-5}}$
B_1 (ppm)	$-1.30\times10^{-4}\,^{+1.34\times10^{-5}}_{-1.34\times10^{-5}}$	$-4.70\times10^{-4}\,^{+2.35\times10^{-4}}_{-4.27\times10^{-4}}$	$1.14\times10^{-4}\,^{+2.29\times10^{-5}}_{-3.47\times10^{-5}}$
A_2 (ppm)	$3.54\times10^{-7}\,^{+8.81\times10^{-6}}_{-8.95\times10^{-6}}$	$-1.96\times10^{-5}\,^{+2.49\times10^{-5}}_{-2.09\times10^{-5}}$	$2.88\times10^{-6}\,^{+1.09\times10^{-5}}_{-1.07\times10^{-5}}$
B_2 (ppm)	$1.03\times10^{-6}\,^{+1.09\times10^{-5}}_{-1.08\times10^{-5}}$	$-2.99\times10^{-5}\,^{+2.89\times10^{-5}}_{-2.64\times10^{-5}}$	$-6.87\times10^{-6}\,^{+1.29\times10^{-5}}_{-1.26\times10^{-5}}$
A_3 (ppm)	$6.72\times10^{-6}\,^{+9.37\times10^{-6}}_{-9.04\times10^{-6}}$	$-9.55\times10^{-7}\,^{+2.58\times10^{-5}}_{-2.64\times10^{-5}}$	$-3.49\times10^{-6}\,^{+1.11\times10^{-5}}_{-1.10\times10^{-5}}$
B_3 (ppm)	$-1.93\times10^{-5}\,^{+1.24\times10^{-5}}_{-1.22\times10^{-5}}$	$-1.05\times10^{-5}\,^{+4.69\times10^{-5}}_{-4.90\times10^{-5}}$	$2.34\times10^{-5}\,^{+1.44\times10^{-5}}_{-1.49\times10^{-5}}$
Π (hr)	—	—	—
α (ppm)	—	—	—
β (ppm)	—	—	—

Table 2: Best-fit parameters for each planet. BTJD stands for Barycentric *TESS* Julian Date, the time unit used by *TESS*. It corrects for orbital motion of Earth, planetary motion, and relativistic effects. Stellar pulsations only apply for KELT-9b.

KELT-9b

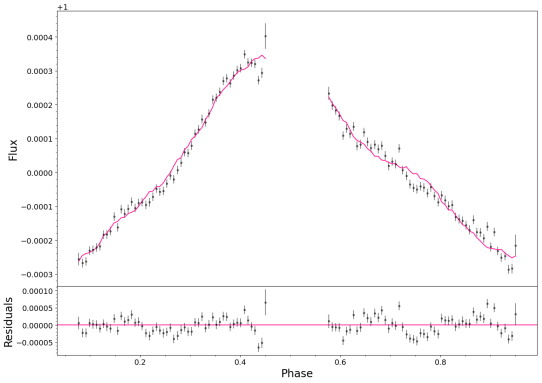

KELT-20b

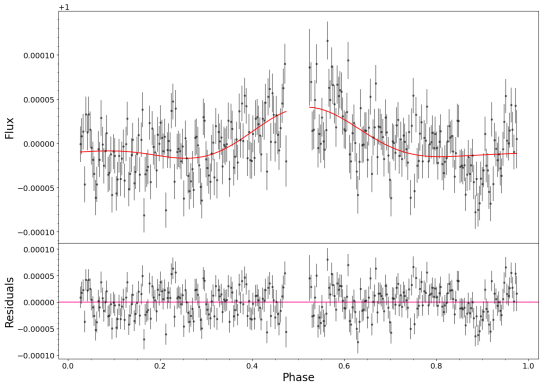

TOI-1431b

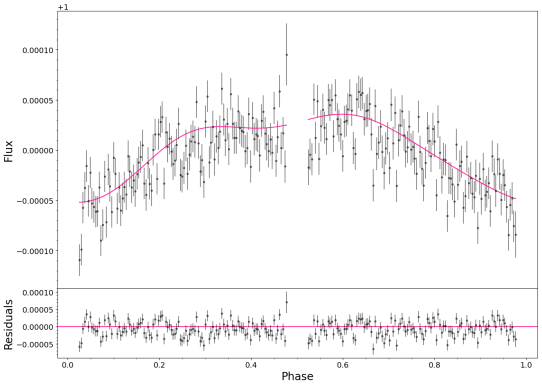

TOI-1518b

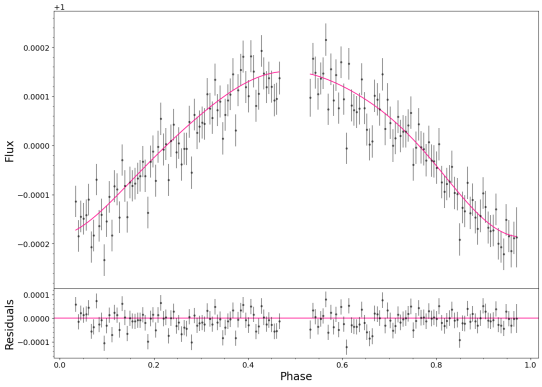

WASP-76b

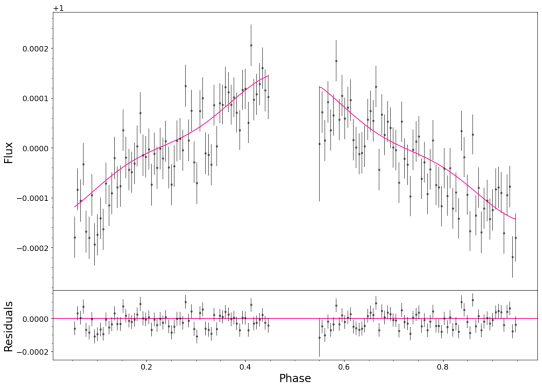

WASP-12b

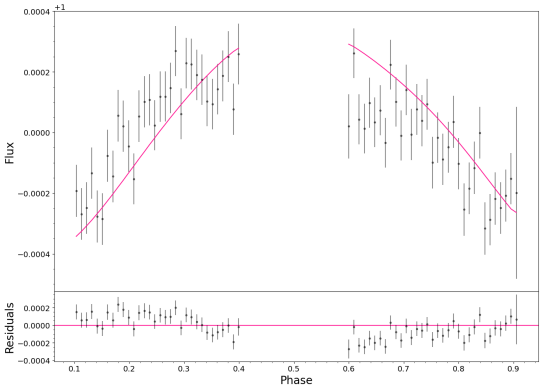

MASCARA-1b

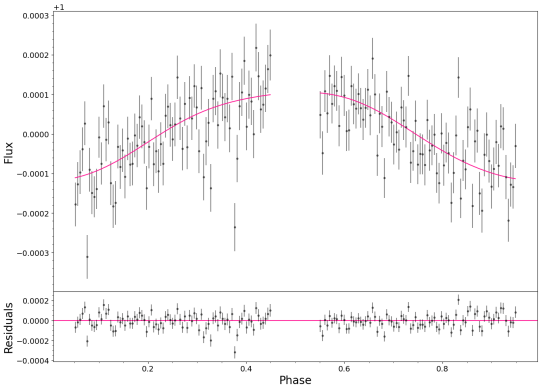

Figure 8: Models of all sectors of data for each exoplanet. Phase-folded light curve represented by black data points. Model represented by pink curve. Residuals underneath each graph with a horizontal pink like at 0 for comparison.

6 References

Exploring the Atmospheric Dynamics of the Extreme Ultrahot Jupiter KELT-9b Using TESS Photometry, Wong et al. 2020

Exoplanet Phase Curves: Observations and Theory, Parmentier and Crossfield 2018

The Astrophysics of Visible-light Orbital Phase Curves in the Space Age, Shporer 2017

Visible-light Phase Curves from the Second Year of the TESS Primary Mission, Wong et al. 2021

The Transiting Exoplanet Survery Satellite, Ricker et al. 2014

Dynesty: A Dynamic Nested Sampling Package, Speagle 2020